Applied Catalysis B: Environmental 113–114 (2012) 141–149

Contents lists available at SciVerse ScienceDirect

Applied Catalysis B: Environmental

journal homepage: www.elsevier.com/locate/apcatb

Fullerene modification CdS/TiO_2 to enhancement surface area and modification of photocatalytic activity under visible light

Ze-Da Meng[a], Mei-Mei Peng[b], Lei Zhu[a], Won-Chun Oh[a,*], Feng-Jun Zhang[c]

[a] Department of Advanced Materials Science & Engineering, Hanseo University, Seosan-si, 356-706, Chungnam-do, Republic of Korea
[b] Chemical Engineering Department, Hanseo University, Seosan, 360-706, Republic of Korea
[c] School of Material Science & Chemical Engineering, Anhui University of Architecture, 230022, P. R. China

ARTICLE INFO

Article history:
Received 23 June 2011
Received in revised form 8 November 2011
Accepted 20 November 2011
Available online 30 November 2011

Keywords:
CdS-C_{60}/TiO_2
FTIR
Visible light
UV–vis
TEM

ABSTRACT

C_{60}-TiO_2, CdS-TiO_2 and CdS-C_{60}/TiO_2 composites were prepared using a sol–gel method, and their photocatalytic activity was evaluated by measuring the degradation of methylene blue (MB) solutions under visible light. The surface area, surface structure, crystal phase and elemental identification of these composites were characterized by nitrogen adsorption isotherms, scanning electron microscopy (SEM), Transmission electron microscopy (TEM), X-ray diffraction (XRD), energy dispersive X-ray spectroscopy (EDX) and UV–vis absorption spectra (UV–vis). XRD showed that the CdS-C_{60}/TiO_2 composite contained a typical single and clear anatase phase. SEM of the CdS-C_{60}/TiO_2 composites revealed a homogenous composition in the particles. EDX revealed the presence of C and Ti with strong Cd and S peaks in the CdS-C_{60}/TiO_2 composite. The degradation of dye was determined by UV–vis spectrophotometry. An increase in photocatalytic activity was observed and attributed to an increase in the photo-absorption effect by fullerene and the cooperative effect of the CdS. The advisable advance BET surface area can enhance the photo-degradation effect. The repeatability of photocatalytic activity was also tested in order to investigate the stability of C_{60} and CdS-C_{60}/TiO_2 composites.

1. Introduction

The photocatalytic degradation of various organic and inorganic pollutants using semiconductor powder as a photocatalyst has been studied extensively [1–3]. TiO_2 is the most widely used photocatalyst for the effective decomposition of organic compounds in air and water under UV irradiation with a wavelength shorter than its band gap energy owing to its relatively high photocatalytic activity, biological and chemical stability, low cost, non-toxic nature and long-term stability [4,5]. On the other hand, the photocatalytic activity of TiO_2 (the band gap of anatase TiO_2 is 3.2 eV and can be excited by photons with <387 nm) is limited to irradiation wavelengths in the UV region. Therefore, only approximately 3–5% of the solar spectrum falls can be used [6], which limits the efficient utilization of solar energy for TiO_2. Some problems still remain to be solved regarding its application, such as the fast recombination of photogenerated electron–hole pairs [7,8]. Therefore, improving the photocatalytic activity by modification has become a hot topic in recent years. Transition metal or non-metal atom-doped TiO_2 or metal complex sensitized TiO_2 have been developed to improve the response of TiO_2 to visible light [9–11].

In recent years, semiconductor coupled TiO_2 systems have been studied extensively in photoelectrochemistry and water splitting systems [12–14]. For example, crystalline cadmium sulfide (CdS) has a smaller band gap energy (2.42 eV) and can be used to induce photocatalytic water decomposition [15]. The potential applications of the photoconductor, CdS, have been demonstrated. It would be desirable to prepare TiO_2 directly particles with homogeneously dispersed CdS because the direct formation of these two semiconductors would provide strong coupling between them [16–18].

Among these materials, carbon supported TiO_2 catalysts have attracted increasing attention [19,20]. C_{60} has interesting properties owing to the delocalized conjugated structures and electron-accepting ability. One of the most remarkable properties of C_{60} in the electron-transfer processes is that it can efficiently arouse rapid photoinduced charge separation and relatively slow charge recombination [21]. Therefore, a combination of photocatalysts and C_{60} might provide an ideal system for enhancing charge separation by photoinduced electron transfer. Some fullerene-donor linked molecules on an electrode have been reported to exhibit excellent photovoltaic effects upon photo-irradiation [22–24].

A conjugated two-dimensional π-system is suitable not only for synthetic light-harvesting systems, but also for efficient electron transfer because the uptake or release of electrons results in minimal structural and solvation changes upon electron transfer.

* Corresponding author.
E-mail address: wc_oh@hanseo.ac.kr (W.-C. Oh).

0926-3373/$ – see front matter © 2011 Elsevier B.V. All rights reserved.
doi:10.1016/j.apcatb.2011.11.031

Table 1
Nomenclatures of the samples prepared with the composites.

Preparation method	Nomenclatures
MCPBA + benzene + C_{60} + TNB	C_{60}-TiO_2
0.008 mol $(CH_3COO)_2Cd{\cdot}2H_2O$ + 0.008 mol Na_2S + TNB	CdS-TiO_2
MCPBA + benzene + C_{60} + 0.008 mol $(CH_3COO)_2Cd{\cdot}2H_2O$ + 0.008 mol Na_2S + TNB	CdS-C_{60}/TiO_2

Fullerenes contain an extensively conjugated three-dimensional π system, and are described as having a closed-shell configuration consisting of 30 bonding molecular orbitals with 60 π-electrons. This material is also suitable for efficient electron transfer reduction because of the minimal changes in structure and solvation associated with electron transfer [25,26].

Fullerene is a promising material because of its band gap (1.6 – 1.9 eV). It has strong absorption in the ultraviolet region and weak but significant bands in the visible region. Fullerene films exhibit fairly high photosensitivity, and fullerene-based solids have been discussed as prospective materials for photovoltaic cells. Heterojunctions of fullerene with many organic semiconductors or conductive polymers have promising photovoltaic effects. Fullerene is an n-type semiconductor, whereas many organic semiconductors are p-type. Therefore, a p–n junction can be formed by fabricating organic semiconductors/fullerene in contact. On the other hand, the quantum efficiencies of these devices are considerably lower than unity [27–29].

During the photo-degradation processes, the strength of the adsorption capacity for dye molecules is also important. Within the limits of the degradation ability, an enhanced adsorption capacity can increase the degradation effect. Fullerenes have relatively larger pore sizes and pore volumes, and are attracting extensive attention for their range of interesting properties owing to their delocalized conjugated structures and electron-accepting ability. Therefore, fullerene in the electron-transfer processes can efficiently arouse rapid photoinduced charge separation and relatively slow charge recombination.

In this paper, CdS-treated TiO_2, fullerene-supported TiO_2 and CdS-C_{60}/TiO_2 were synthesized and exhibited enhanced vis-photocatalytic activity compared to pure TiO_2. This study focused on the fabrication and characterization of CdS-C_{60}/TiO_2 composite in a preparation procedure. The structural variations, surface state and elemental compositions were examined for the preparation of CdS-C_{60}/TiO_2 composites. X-ray diffraction (XRD), scanning electron microscopy (SEM), energy dispersive X-ray (EDX), transmission electron microscopy (TEM), nitrogen adsorption isotherms and UV–vis absorption spectra were used to characterize the new photocatalysts. The catalytic efficiency of the CdS-C_{60}/TiO_2 composite was evaluated by measuring the photo degradation of methylene blue (MB, $C_{14}H_{14}N_3NaO_3S$) and methylene orange (MO, $C_{14}H_{14}N_3NaO_3S$).

2. Experimental

2.1. Materials

Crystalline fullerene [C_{60}] powder of 99.9% purity from TCI (Tokyo Kasei Kogyo Co. Ltd., Japan) was used as the carbon matrix. Titanium (IV) n-butoxide (TNB, $C_{16}H_{36}O_4Ti$) as a titanium source for the preparation of the CdS-C_{60}/TiO_2 composites was purchased as reagent-grade from Acros Organics (USA). Cadmium acetate dehydrate [$(CH_3COO)_2Cd{\cdot}2H_2O$] was supplied by Daejung Chemicals and Metals Co., Ltd (Korea), and Sodium sulfide ($Na_2S{\cdot}5H_2O$) was obtained from Yakuri pure Chemicals. Co., Ltd (Japan). *m*-chloroperbenzoic acid (MCPBA, Acros Organics, New Jersey, USA) was used as an oxidized reagent to oxidize the fullerene surface. Methylene blue (MB, $C_{16}H_{18}N_3SCl{\cdot}3H_2O$) was analytical grade and purchased from Duksan Pure Chemical Co., Ltd. The Methylene Orange (MO, $C_{14}H_{14}N_3NaO_3S$, 99.9%) was purchased from Daejung Chemicals & Metals Co., Ltd, (Korea). Benzene and ethyl alcohol were reagent-grade and purchased from Duksan Pure Chemical Co (Korea) and Daejung Chemical Co. (Korea), and used as received unless otherwise stated.

2.2. Oxidation of C_{60} surface

MCPBA (*m*-chloroperbenzoic acid, ca. 1 g) was suspended in 50 ml benzene, followed by the addition of fullerene [C_{60}] (ca. 40 mg). The mixture was heated under reflux in air and stirred for 6 h. The solvent was then dried at the boiling point of benzene (353.13 K). After completion, the dark brown precipitates were washed with ethyl alcohol and dried at 323 K, and C_{60} oxidation was performed.

2.3. Preparation of CdS-C_{60}

A stoichiometric amount of 30 ml $(CH_3COO)_2Cd{\cdot}2H_2O$ ethanol solutions (0.26 M, 0.20 M, 0.13 M) were mixed with oxidized C_{60}. With continuous stirring at 343 K, 50 ml of a Na_2S aqueous solution (0.16 M, 0.12 M, 0.08 M) was then added to the mixture dropwise at the rate of 6 drops/min. After stirring for 7 h, the final mixture was then filtered and washed with deionized water. A dark green CdS-C_{60} powder was obtained after heat treatment at 573 K for 1 h.

2.4. Preparation of CdS-C_{60}/TiO_2 composites

CdS-C_{60} was prepared using pristine TNB for the preparation of CdS-C_{60}/TiO_2 composites. CdS-C_{60} powder was mixed with 3 ml TNB. The solutions were then homogenized under reflux at 343 K for 5 h in a vial with constant stirring. After stirring, the solution transformed into CdS-C_{60}/TiO_2 gels, and heat treated at 873 K to produce the CdS-C_{60}/TiO_2 composites. The CdS-TiO_2 composites were prepared using sol–gel methods. Regarding the CdS coating, the nomenclatures of the samples for cadmium acetate dehydrate and sodium sulfide solutions are shown in Table 1.

2.5. Characterization of photocatalysts compounds

To measure the structural variations, the XRD patterns were obtained using an X-ray generator (Shimadzu XD-D1, Japan) with Cu Kα radiation. Scanning electron microscopy (SEM, JSM-5200 JOEL, Japan) was used to observe the surface state and structure of the photocatalyst composites. Energy dispersive X-ray spectroscopy (EDX) was also employed for elemental analysis. Transmission electron microscopy (TEM, JEOL, JEM-2010, Japan) was used to observe the surface state and structure of the photocatalyst composites at an acceleration voltage of 200 kV. TEM was also used to examine the size and distribution of the titanium and iron particles deposited on the fullerene surface of various samples. The TEM specimens were prepared by placing a few drops of the sample solution on a carbon grid. Ultraviolet–visible light spectroscopy (Neosys-2000) was performed using $BaSO_4$ as a reference. The spectra were converted from reflection to absorbance using the Kubelka–Munk method. The nitrogen adsorption–desorption isotherms were measured at 77 K on a Micromeritics ASAP 2010

volumetric adsorption analyzer (Japan). Prior to each adsorption measurement, the samples were evacuated at 200 °C under vacuum ($p < 10^{-5}$ mbar) for 6 h in the degas port.

2.6. Photocatalytic degradation of dye

The photocatalytic activities were evaluated by dye (MB and MO) degradation in aqueous media under visible light irradiation. For visible light irradiation, the reaction beaker was located axially and held in a visible lamp (8 W, halogen lamp, KLD-08L/P/N, Korea) box. The luminous efficacy of the lamp was 80 lm/W, and the wavelength was 400–790 nm. The lamp was used at a distance of 100 mm from the aqueous solution in a dark box. The initial concentration of dye was set to 1×10^{-5} mol/L in all experiments. The amount of the CdS-fullerene/TiO_2 composite was 0.05 g/(50 ml solution). The reactor was placed for 2 h in a dark box to allow the CdS-fullerene/TiO_2 composites particles to adsorb the maximum amount of dye moleculars. After adsorption, the visible light irradiation was restarted to allow the degradation reaction to proceed. In the process of dye degradation, a glass reactor (diameter = 4 cm, height = 6 cm) was used and the reactor was placed on the magnetic churn dasher. The suspension was then irradiated with visible light for a set irradiation time. Visible light irradiation of the reactor was performed for 10 min, 30 min, 60 min, 90 min and 120 min, respectively. The samples were withdrawn regularly from the reactor and the dispersed powders were removed using a centrifuge. The clean transparent solution was analyzed by UV/vis spectroscopy. The dye concentration in the solution was measured as a function of the irradiation time.

2.7. Circle use for composites

The cleaned CdS-C_{60}/TiO_2 composites were immersion in ethanol for 6 h and rinsed with deionized water, and then dried at 353 K. After this the cleaned CdS-C_{60}/TiO_2 composites were reused for remove dyes, and the circle experiment is doing several times.

3. Results and discussion

3.1. FTIR spectra of compounds

The FTIR spectrum of C_{60} was rather simple and suggested extensive oxidation. The spectra of the crystalline material showed well distinguished and sharp bands, whereas the amorphous spectra were less resolved. The hydration results established the importance of defined conditions for FTIR (Fig. 1) and showed that C_{60} could be oxidized. They also suggested that this type of study can be performed on oxidized C_{60}. Fig. 1(a)–(c) shows the FTIR spectrum of oxidized C_{60}, CdS-C_{60} and CdS-C_{60}/TiO_2, respectively. The FTIR spectrums of samples were similar to that of oxidized C_{60}.

From Fig. 1(a), the peak at 671 cm^{-1} was assigned to alkane bending vibration, which is between 650 and 1000 cm^{-1}, and the peaks at 705, 752 and 807 cm^{-1} were assigned to aromatic symmetric stretching modes, which are between 690 and 900 cm^{-1}. A strong C–O band at approximately 1253 and 1288 cm^{-1}, and a strong C=C band at 1475 cm^{-1} were observed. The functional groups, C=O and C–OH, were indicated in the spectrum at approximately 1693, 1797 and 1072 cm^{-1}. –OH was observed at approximately 1407 cm^{-1}.

This confirms that artificial ageing is actually occurring in the exposed film, and that the types of structural changes inferred from the spectra are consistent with the mechanism proposed in the literature: the formation of O–H bonds resulting from the oxidation of the hydrocarbon triterpenic molecules by the direct binding of O• and O–O radicals, followed by further oxidation to carbonylic functions.

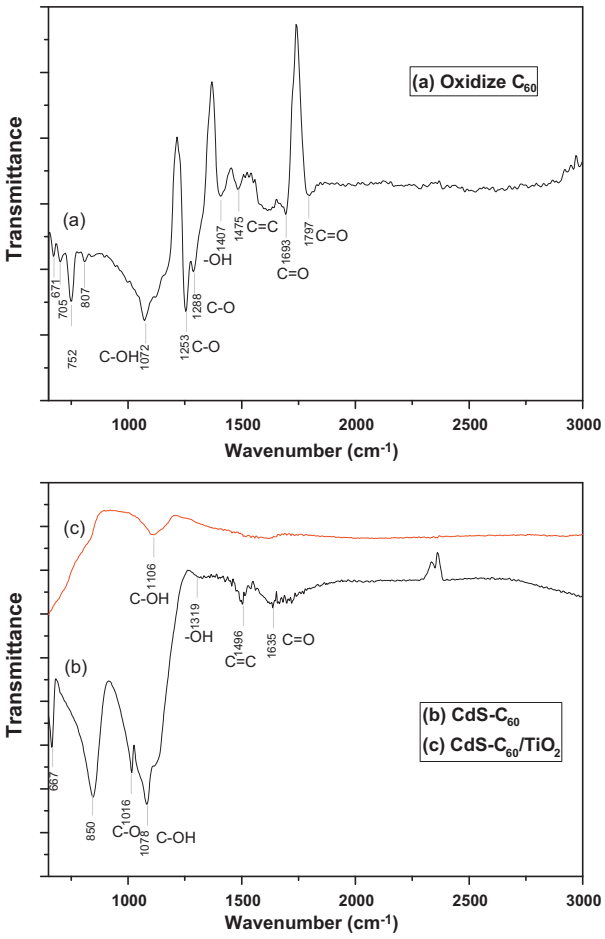

Fig. 1. FTIR spectra of oxidized C_{60}, CdS-C_{60} and CdS0C_{60}/TiO_2.

In Fig. 1(b), the peak at 667 cm^{-1} was assigned to alkane bending vibration, which is between 650 and 1000 cm^{-1}, and a peak corresponding to the aromatic symmetric stretching modes at 850 cm^{-1} was observed. The strong peak at 1016 cm^{-1} and the week peak at 1496 cm^{-1} was assigned to C–O band and C=C band, respectively. A broad stretch at 1319 was assigned to –OH band. The C–OH and C=O functional groups were observed at approximately 1078 and 1635 cm^{-1}, respectively. Compared to the spectrum curves (a), (b) and (c), the peak intensity of the functional group on oxidized C_{60} was weak and decreased and the amount of the functional group was decreased. This is because some of the functional groups had combined with CdS and TiO_2 particles. The CdS and TiO_2 particles were bound to fullerene with different functional groups.

3.2. Elemental analysis of the preparation

Fig. 2 shows the energy dispersive X-ray spectra of the surface of the CdS-TiO_2, CdS-C_{60} and CdS-C_{60}/TiO_2 compounds. The elemental composition of these samples was analyzed and the characteristic elements were identified using an EDX detection spectrometer. Fig. 2 shows that strong Kα and Kβ peaks from the Ti element appear at 4.51 and 4.92 keV, respectively, whereas a moderate Kα peak for O was observed at 0.52 keV [30]. In addition to the above peaks, S and Cd were also found. In Fig. 2, quantitative microanalysis of C, O, Ti, Cd and S, as the major elements for the composites were performed by EDX. From the EDX data, the main elements, such as C, O, Ti, Cd and S, were observed. Table 2 lists the results of EDX quantitative microanalysis of the samples. In Fig. 2(c), the spectra show the presence of C, O and Ti, as major elements, with strong

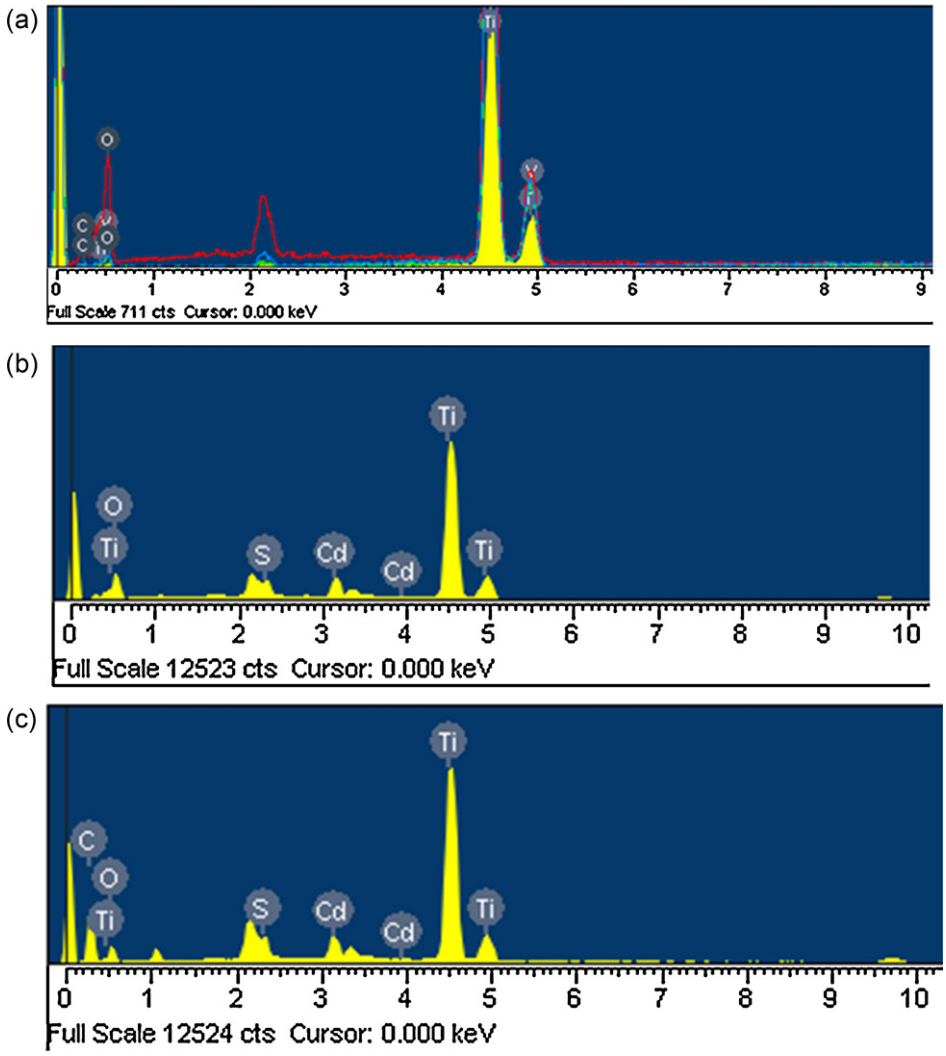

Fig. 2. EDX elemental microanalysis of C_{60}-TiO_2 (a), CdS-TiO_2 (b) and CdS-C_{60}/TiO_2 (c).

Cd and S peaks. Some small impurities were observed, which were considered to have been introduced into the composites using the fullerene without purification. In most samples, carbon and titanium were present as the major elements with small quantities of oxygen in the composite.

3.3. Surface characteristics of the samples

Fig. 3 shows the characterization of the micro-surface structures and morphology of the C_{60}-TiO_2, CdS-TiO_2 and CdS-C_{60}/TiO_2 compounds. Fig. 3 shows that C_{60} and CdS are coated uniformly on the TiO_2 surface, which leads to an increase in nanoparticle size. Zhang et al. reported that a good dispersion of small particles could provide more reactive sites for the reactants than aggregated particles [31]. The surface roughness appears to be more with little grain aggregation. In Fig. 3, (a) is C_{60}-TiO_2, (b) is CdS-TiO_2 and (c) is CdS-C_{60}/TiO_2. The aggregation phenomenon becomes increasingly serious, and the CdS addition can make the aggregation worse. Fig. 3(a) shows spherical C_{60} particles. No spherical particles were observed in Fig. 3(c), even though this is due to partial agglomeration forming block particles.

Table 2 lists the BET surface areas of the raw C_{60}-TiO_2, CdS-TiO_2 and CdS-C_{60}/TiO_2 photocatalyst. The BET value decreased from 85.00 m^2/g of pure fullerene to 41.67 m^2/g of CdS-C_{60}/TiO_2. The TiO_2 and CdS particles were introduced into the pores of fullerene, and the value of CdS-C_{60}/TiO_2 decreased. The C_{60}-TiO_2 sample had a larger surface area that can affect the adsorption reaction [32]. Added C_{60} can increase the surface area because C_{60} has a relatively larger surface area. The BET value of CdS-TiO_2 and the C_{60} modified CdS-TiO_2 compounds was 26.71 m^2/g and 41.67 m^2/g, respectively. The BET surface area of the CdS-TiO_2 photocatalyst was increased by 56.00% when the CdS-TiO_2 particles are modified by C_{60}. The

Table 2
EDX elemental microanalysis, BET surface area values and K_{app} values of the photocatalysts.

Sample name	C (%)	O (%)	Cd (%)	S (%)	Ti (%)	BET (m^2/g)	K_{app}
C_{60}	99.99	-	-	-	-	85.05	–
TiO_2	-	-	-	-	99.99	18.95	2.24×10^{-4}
C_{60}-TiO_2	4.12	42.41	-	-	53.47	80.25	5.43×10^{-3}
CdS- TiO_2	-	40.32	8.71	1.32	-	26.71	1.61×10^{-3}
CdS-C_{60}/TiO_2	4.99	57.42	0.79	0.24	35.33	41.67	7.90×10^{-3}

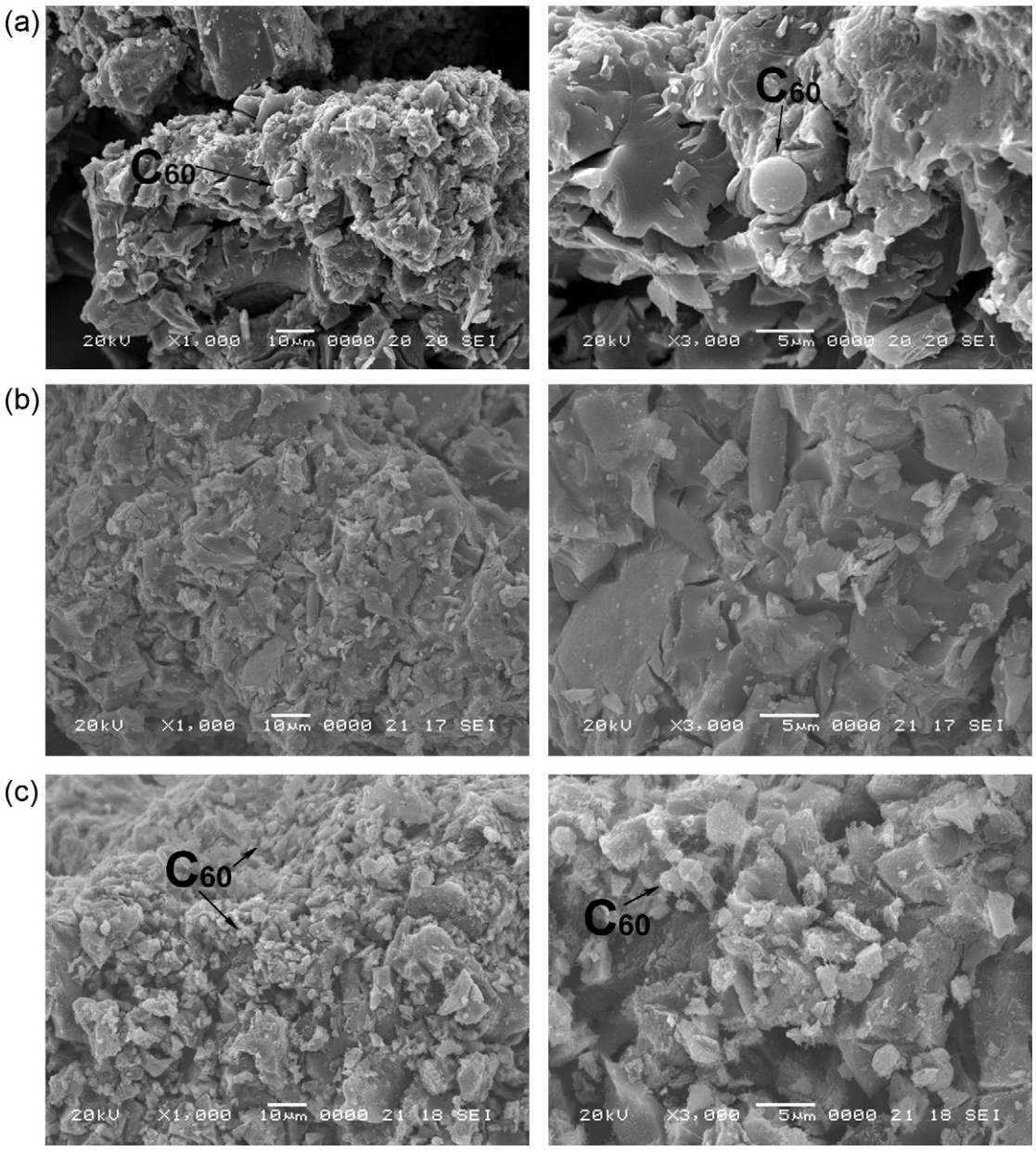

Fig. 3. SEM images of C_{60}-TiO_2 (a), CdS-TiO_2 (b) and CdS-C_{60}/TiO_2 (c).

pore size and pore volume increased significantly when the particles were modified by C_{60} because C_{60} particles have a larger surface area and pores.

Fig. 4 shows the adsorption isotherm of N_2 at 77 K for CdS-TiO_2 and CdS-C_{60}/TiO_2 compounds. The isotherms belong to a mixed type in the IUPAC classification. Type II Adsorption Isotherm shows large deviations from the Langmuir model of adsorption. The intermediate flat region in the isotherm corresponds to monolayer formation. The type II isotherms do not exhibit a saturation limit as Type I. This type of isotherm indicates indefinite multi-layer formation after the completion of the monolayer and is found in adsorbents with a wide range of pore sizes. A monolayer is completed close to the first point of inflexion (point A), after which adsorption occurs in successive layers. Compared to the adsorption effect of catalyst with or without C_{60}, the special surface area increased when CdS/TiO_2 compounds were modified with C_{60}. The adsorption effect of CdS-C_{60}/TiO_2 is approximately 2 times for CdS/TiO_2. From Fig. 4, added C_{60} can enhance the BET surface area, which can increase the adsorption effect.

Fig. 5 shows TEM images of CdS-C_{60}/TiO_2. The representative TEM images in Fig. 5 show that the prepared powders are uniform with some aggregations between particles. The mean diameter of C_{60} was estimated to be approximately 20 nm. From Fig. 5, the image of CdS-C_{60}/TiO_2 compounds showed that all particles had agglomerated. This suggests that the presence of CdS and C_{60} can efficiently enhance the agglomeration of TiO_2 and impede the dispersion of nanoparticles.

3.4. Structural analysis

Fig. 6 shows XRD patterns of C_{60}-TiO_2, CdS-TiO_2 and CdS-C_{60}/TiO_2 composites. In Fig. 6, C is the characteristic peaks corresponding to C_{60}, A is anatase and S is CdS. The XRD pattern of the CdS-C_{60} revealed a crystalline phase of C_{60} and CdS. The peaks

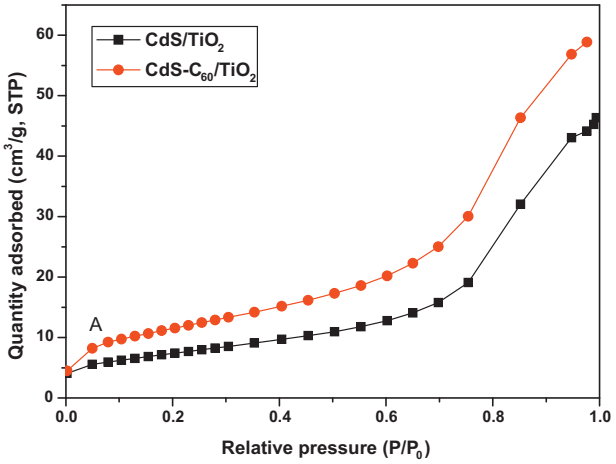

Fig. 4. Nitrogen adsorption isotherms of CdS-TiO_2 and CdS-C_{60}/TiO_2 at 77 K.

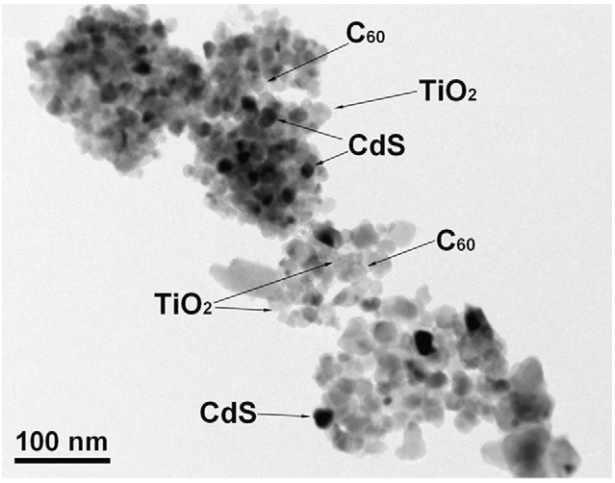

Fig. 5. TEM image of the CdS-C_{60}/TiO_2 compounds.

at 24.7, 26.5, 28.3, 36.6, 43.8, 48.1 and 51.8° 2θ were assigned to the (1 0 0), (0 0 2), (1 0 1), (1 0 2), (1 1 0), (1 0 3) and (1 1 2) planes of the hexagonal structure of CdS [33,34]. The XRD patterns of CdS-C_{60}/TiO_2 also showed CdS peaks at 28.3, 43.8 and 51.8° 2θ, which were assigned to the (1 0 1), (1 1 0) and (1 1 2) planes of the hexagonal structure of CdS due to the presence of a small amount of CdS

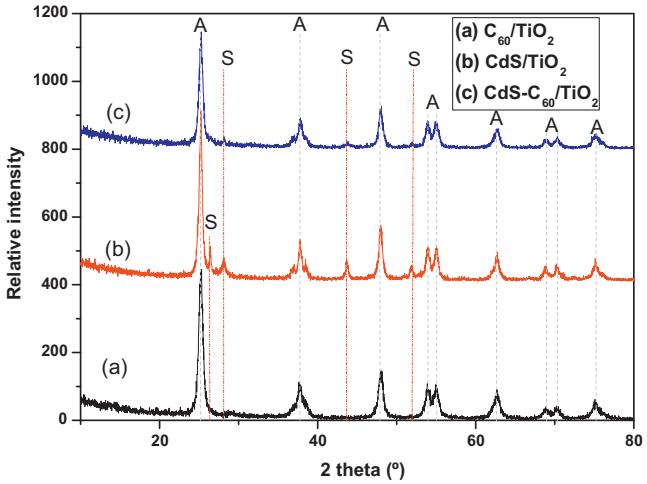

Fig. 6. XRD patterns of C_{60}-TiO_2 (a), CdS-TiO_2 (b) and CdS-C_{60}/TiO_2 (c).

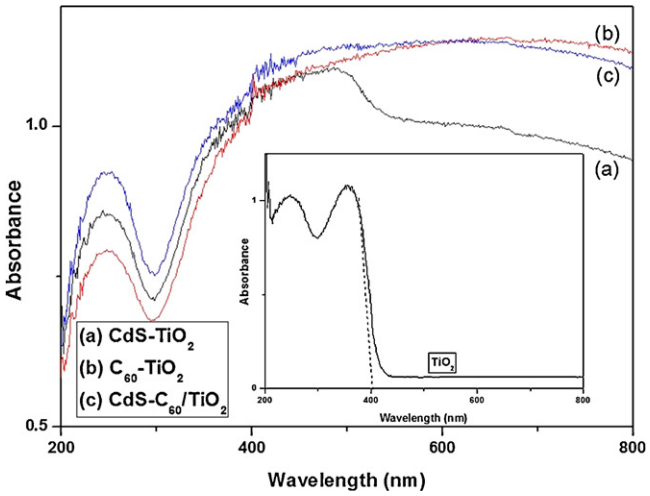

Fig. 7. UV–vis absorption spectra of the photocatalysts.

on the TiO_2, which can reduce the intensity of the peaks related to the CdS, and the interference of TiO_2 peaks. The CdS content was only approximately 1%, as determined by EDX. The XRD patterns of C_{60}-TiO_2 showed a crystalline phase of TiO_2, the peaks for C_{60} could not be found due to the presence of a small amount of C_{60} and the interference of TiO_2. The major peaks at 25.3, 37.5, 48.0, 53.8, 54.9, 62.5, 68.7, 70.3, 75.1 and 82.6° 2θ were assigned to the (1 0 1), (0 0 4), (2 0 0), (1 0 5), (2 1 1), (2 0 4), (1 1 6), (2 2 0), (2 1 5) and (2 2 4) planes of anatase, which indicate that the prepared TiO_2 is anatase [35,36]. A comparison of the XRD patterns of CdS-TiO_2 and CdS-C_{60}/TiO_2 revealed a decrease in the intensity of the TiO_2 peak in CdS-C_{60}/TiO_2 and peak at 82.6° 2θ. Therefore, of the introduction of CdS prevented the growth of anatase.

3.5. UV–vis diffuse reflectance spectroscopy

Fig. 7 shows the UV–vis absorption spectra of the samples. The inset shows the UV–vis absorption spectrum for pure TiO_2. TiO_2, C_{60}-TiO_2, CdS-TiO_2 and CdS-C_{60}/TiO_2 composites showed great absorption in ultraviolet region, but the absorption edge of TiO_2 was approximately 400 nm (E_g = 3.2 eV). In the visible region, the C_{60}-TiO_2, CdS-TiO_2 and CdS-C_{60}/TiO_2 composites showed has good absorption, which means that these composites have great photocatalytic activity under visible light irradiation. Because CdS has a smaller band gap (2.42 eV) and can be used to induce photocatalysis, CdS-TiO_2 has good adsorption in the visible region. In the case of C_{60} coupled TiO_2, C_{60} acted as a photosensitizer, which could be excited to inject electrons into the conduction band of TiO_2. The adsorption effect of CdS-C_{60}/TiO_2 is good at visible region because of the synergistic reaction of CdS, C_{60} and TiO_2. The absorption effect of CdS-TiO_2 in the visible region decreased when the wavelength is approximately 550 nm [37,38].

3.6. Photocatalytic activity of samples

Fig. 8 shows the time series of dye degradation using C_{60}-TiO_2, CdS-TiO_2 and CdS-C_{60}/TiO_2 under visible light irradiation. The spectra for the dye solution after visible light irradiation show the relative degradation yields at different irradiation times. The decrease in dye concentration continued with an oppositely gentle slope, which was due to visible light irradiation. In Fig. 8(a)–(c) are the degradation for MB solution, (d) is the degradation for MO solution. The concentration of dyes was 1.0×10^{-5} mol/L, the absorbance for dye decreased with increasing visible light irradiation time. Moreover, the dye solution increasingly lost its color,

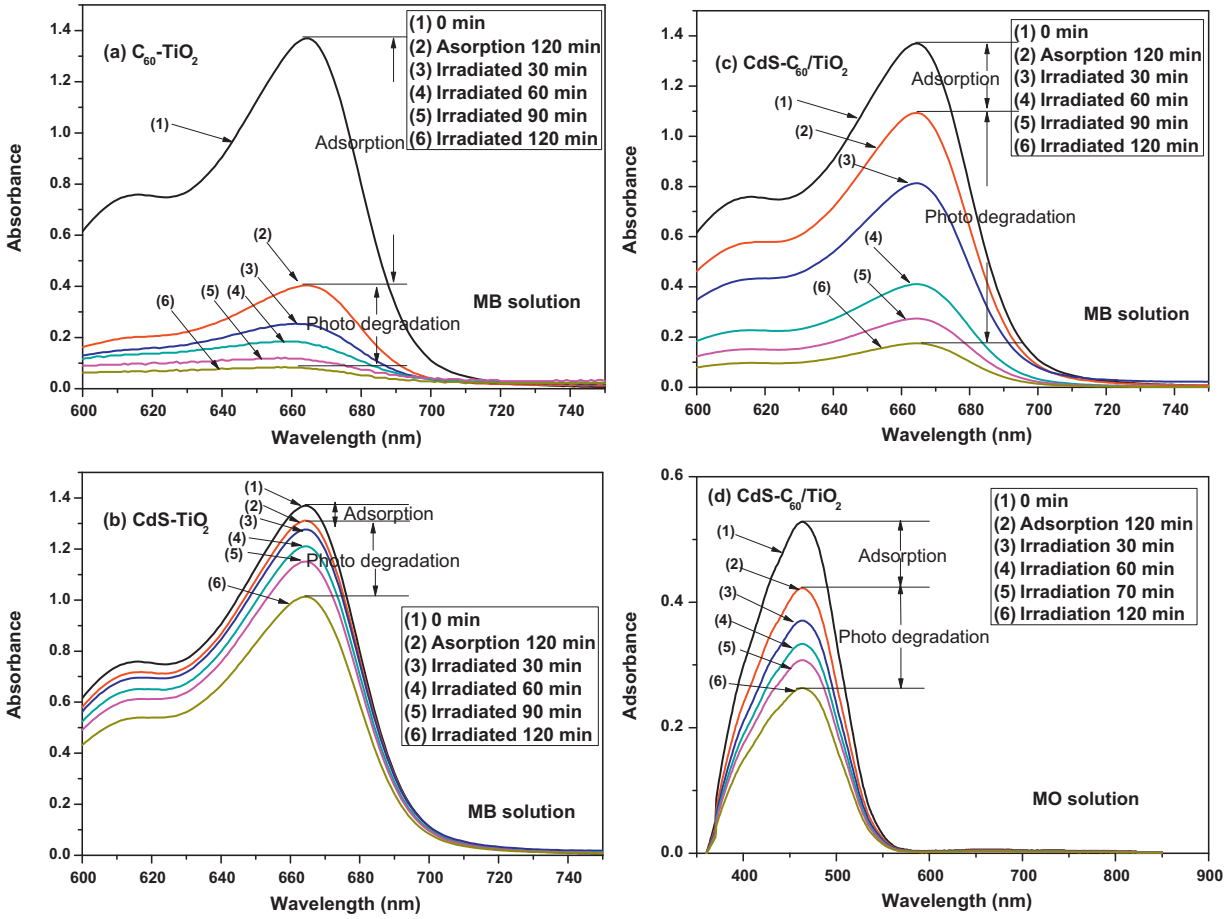

Fig. 8. UV–vis spectra of the MB concentration against C_{60}-TiO_2 (a), CdS-TiO_2 (b) and CdS-C_{60}/TiO_2 (c). Composites as a function of time and MO concentration against CdS-C_{60}/TiO_2 (d).

and the dye concentration continued to decrease. Two steps are involved in the photocatalytic decomposition of dyes; the adsorption of dye molecules and degradation. After adsorption in the dark for 2 h, the samples reached adsorption–desorption equilibrium. In the adsorptive step, TiO_2, C_{60}-TiO_2, CdS-TiO_2 and CdS-C_{60}/TiO_2 composites showed different adsorptive effects with C_{60}-TiO_2 having the best adsorptive effect. The adsorptive effect of pure TiO_2 was the lowest. The adsorptive effect of CdS-C_{60}/TiO_2 was better than that of CdS-TiO_2 because the added C_{60} can enhance the BET surface area which can increase the adsorption effect. C_{60}-TiO_2 has the largest BET surface area, which can enhance the adsorptive effect. In the degradation step, the CdS-TiO_2, C_{60}-TiO_2 and CdS-C_{60}/TiO_2 composites showed a good degradation effect, as shown in the UV–vis absorption spectra. The CdS-C_{60}/TiO_2 composites

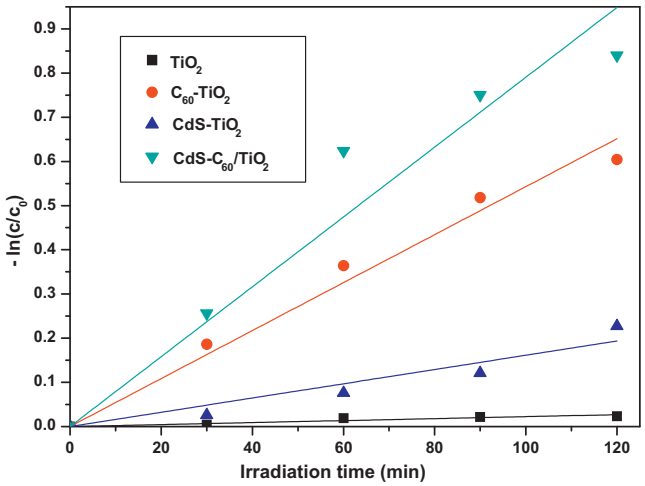

Fig. 9. Corresponding $-\ln(C/C_0)$ vs. t plots.

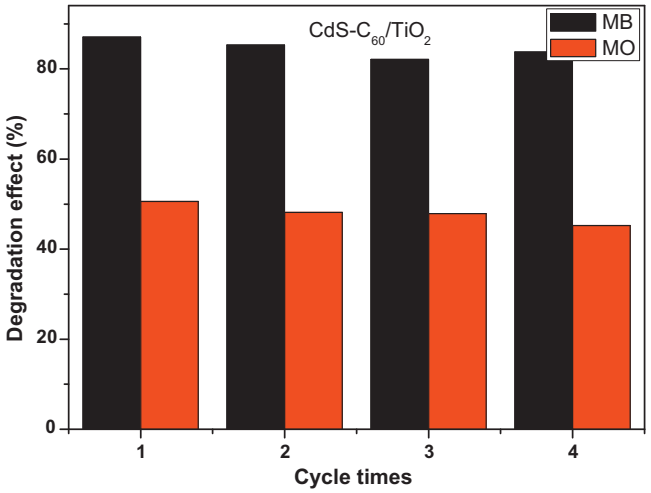

Fig. 10. Reuse experiment for CdS-C_{60}/TiO_2 composites.

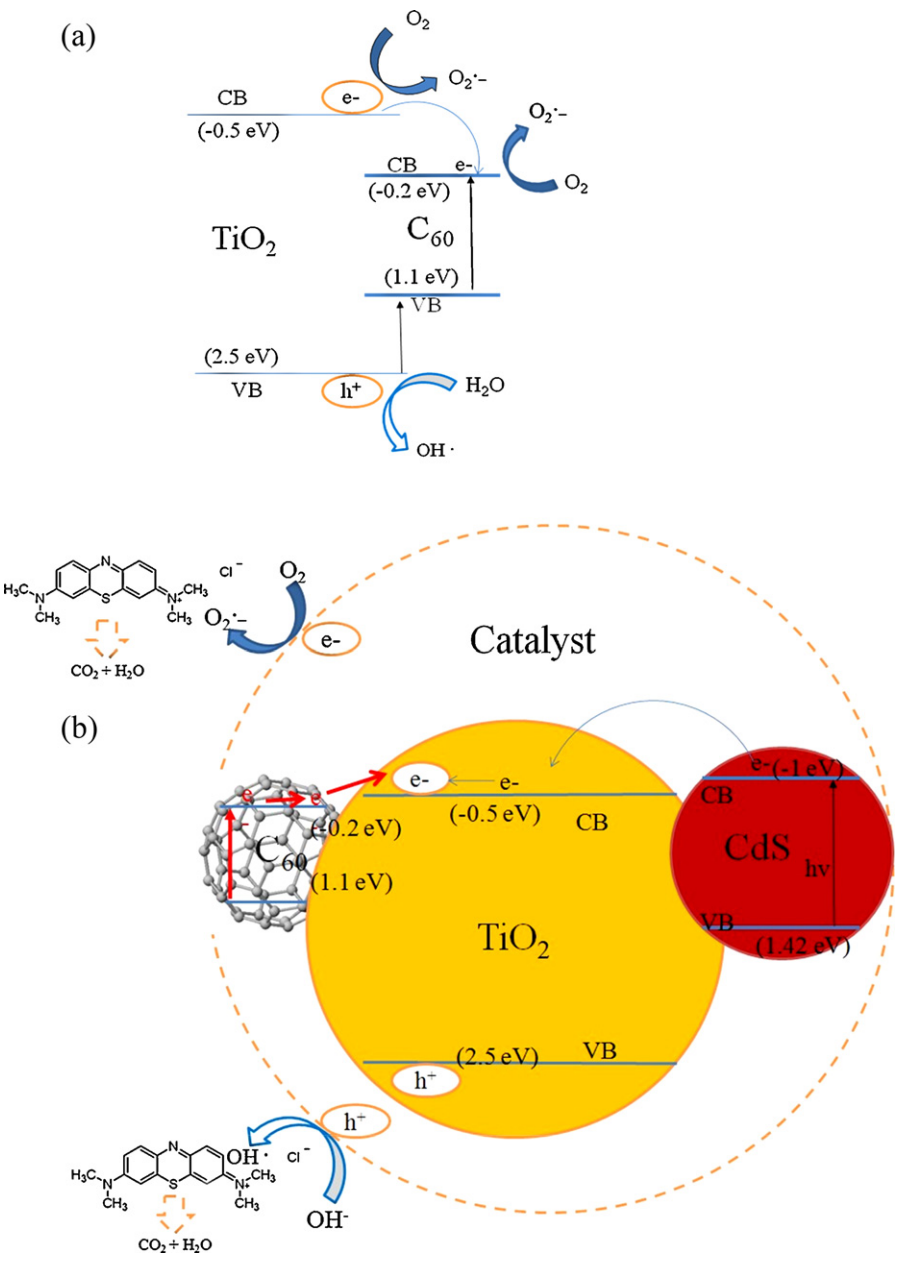

Fig. 11. Schematic diagram of the separation of generated electrons and holes on the interface of C_{60}-TiO_2 (a) and CdS-C_{60}/TiO_2 (b) compounds under visible light irradiation.

showed good adsorption and degradation effects. A comparison of the decoloration effect of the catalysts showed that the degradation effect can be increased by an increase in the adsorption capacity.

Fig. 9 shows the $-\ln(C/C_0)$ vs. t plots at 0–120 min irradiation time. The photodegradation followed first-order kinetics, which can be expressed as follows: $-\ln(C/C_0) = k_{app}t$, where k_{app} is the apparent reaction rate constant, C_0 and C are the initial and reaction concentration of MB, respectively. Table 2 lists the rate constant (k_{app}) of pure TiO_2, C_{60}-TiO_2, CdS-TiO_2 and CdS-C_{60}/TiO_2 composites for the degradation of the MO solution. The k_{app} value of the CdS-C_{60}/TiO_2 sample was the largest, which is in accordance with the photocatalytic activity.

To evaluate the photochemical stability of the catalyst, the repeated experiments for the photocatalytic decomposition of dyes were performed CdS-C_{60}/TiO_2 samples, and the results are shown in Fig. 10. As shown in Fig. 10 the reused CdS-C_{60}/TiO_2 sample does not show apparent change in photocatalytic activity, which emphasizes the excellent photochemical stability of the C_{60} and C_{60} modified photocatalyst. C_{60} modification can not only improve the photocatalytic performance but also long-term stability of TiO_2 nanocrystals. This result is significant from the viewpoint of practical application, as the enhanced photocatalytic activity and prevention of catalyst deactivation will lead to more cost-effective operation.

C_{60}-TiO_2 has a better degradation effect than pure TiO_2 because fullerene is an energy sensitizer that improves the quantum efficiency and increases the level of charge transfer. According to an earlier study [39], dye molecules absorb energy from irradiation, which shift their delocalized electrons from bonding to antibonding orbitals. Since dye adsorption likely occurs via π–π interactions between its delocalized electrons and the graphene layers of carbon, it is reasonable that shifts in its electron orbitals would alter adsorption [40]. The TiO_2 deposited on the C_{60} surface can retain its photo-degradation activity. In the fullerene coupled TiO_2

system, the photocatalytic activity was enhanced mainly by the high efficiency of charge separation induced by the synergistic effect of fullerene and TiO_2. In the case of fullerene-coupled TiO_2, hole and electron pairs were generated and separated on the dinterface of C_{60} by visible light irradiation. The level of the conduction band in TiO_2 was lower than the reduction potential of C_{60} [41]. Therefore, the photogenerated electron can transfer easily from the conduction band of fullerene to a TiO_2 molecule with an interaction between C_{60} and TiO_2. Simultaneously, the holes in the valence band (VB) of TiO_2 can transfer directly to C_{60} because the VB of TiO_2 matches well with C_{60}. The synergistic effect of fullerene and TiO_2 in the C_{60}-hybridized TiO_2 samples promoted the separation efficiency of the photogenerated electron–hole pairs, resulting in high photocatalytic activity [42]. In this case, the C_{60} coupled TiO_2 system improved the reaction state [43]. Therefore, the C_{60} coupled TiO_2 has photocatalytic activity under visible light irradiation. Fig. 11(a) shows a schematic diagram of the separation of photogenerated electrons and holes on the C_{60}-TiO_2 interface.

In the CdS-TiO_2 system, CdS has a relativity smaller band gap (2.42 eV) and can be used to induce photocatalysis with visible light irradiation. In case of the addition of CdS, the electrons excited from the CdS particle are transferred rapidly to a TiO_2 particle because the conduction band of CdS is −1 eV, which is −0.5 more negative than that of TiO_2 [44]. This indicates that the electrons from excited CdS are injected into the conduction band of TiO_2 and are then scavenged by molecular oxygen O_2 to yield the superoxide radical anion O_2^-. Therefore, this vectorial transfer of the change should enhance the photo-oxidation of the adsorbed organic substrate. On the other hand, the photo-generated holes in CdS nanocrystals cannot oxidize hydroxyl groups to hydroxyl radicals due to its valence band potential. This results in the photo-corrosion of CdS, forming cadmium cations [45]. This approach is still pursued to produce a stable CdS photocatalyst.

CdS-C_{60}/TiO_2 composites have the best discoloration effect, which is due the following reasons: (1) C_{60} is an energy sensitizer that improves the quantum efficiency and increases charge transfer; (2) C_{60} can enhance the adsorption effect during the discoloration processes; and (3) CdS can provide excited electrons for TiO_2, and engender hydroxyl radicals ($^{\bullet}OH$) and superoxide radical anions ($^{\bullet}O_2^-$) with the presence of H_2O and oxygen. Fig. 11(b) shows a schematic diagram of the separation of photogenerated electrons and holes on the CdS-C_{60}/TiO_2 interface.

4. Conclusions

Photocatalysts were synthesized successfully using a simple sol–gel method. From the XRD patterns, the cubic crystal structure of CdS was observed. TEM showed that the surface of TiO_2 has been coated uniformly with C_{60} and CdS layers with a C_{60} particle size of approximately 20 nm. The diffuse reflectance spectra indicated that the composites showed strong photoabsorption in the UV and visible range, and presence of C_{60} enhanced the level of photoabsorption in the visible range. The nitrogen adsorption isotherms show that added C_{60} can enhance the adsorption effect significantly. The photocatalytic activity of the CdS-C_{60}/TiO_2 composite was examined by the degradation of MB in aqueous solutions under visible light irradiation. The CdS-C_{60}/TiO_2 composites showed good adsorption and degradation effects. Overall, within the limits of the degradation ability, the degradation effect can be enhanced by an increase in adsorption capacity. CdS-C_{60}/TiO_2 composite also have good photocatalytic activity in cycles experiment which emphasizes the excellent stability of the C_{60} and photochemical stability of C_{60} modified photocatalyst.

References

[1] E. Piera, M.I. Tejedor, M.E. Zorn, M.A. Anderson, Appl. Catal. B: Environ. 47 (2004) 219–256.
[2] P. Calza, V.A. Sakkas, C. Medana, C. Baiocchi, A. Dimou, E. Pelizzetti, T. Albanis, Appl. Catal. B: Environ. 67 (2006) 197–205.
[3] C.G. Silva, W. Wang, J.L. Faria, J. Photochem. Photobiol. A 181 (2006) 314–324.
[4] V. Shah, P. Verma, P. Stopka, J. Gabriel, P. Baldrian, F. Nerud, Appl. Catal. B: Environ. 46 (2003) 287–292.
[5] T. Sauer, G. Cesconeto Neto, H.J. Jose, R.F.P.M. Moreira, J. Photochem. Photobiol. A: Chem. 149 (2002) 147–154.
[6] W.C. Oh, J.H. Son, F.J. Zhang, M.L. Cheng, J. Korean Ceram. Soc. 46 (2009) 1–9.
[7] Z.D. Meng, K. Zhang, W.C. Oh, Korean J. Mater. Res. 20 (2010) 228–234.
[8] R. Asahi, T. Morikawa, T. Ohwaki, K. Aoki, Y. Taga, Science 293 (2001) 269–271.
[9] V. Pore, M. Ritala, M. Leskela, S. Areva, M. Jarn, J. Jarnstrom, J. Mater. Chem. 17 (2007) 1361–1371.
[10] Z.D. Meng, L. Zhu, J.G. Choi, M.L. Chen, W.C. Oh, J. Mater. Chem. 21 (2011) 7596–7603.
[11] D. Dvoranova, V. Brezova, M. Mazur, M.A. Malati, Appl. Catal. B: Environ. 37 (2002) 91–105.
[12] Y. Bessekhouad, D. Robert, J.V. Weber, J. Photochem. Photobiol. A 163 (2004) 569–580.
[13] Y. Bessekhouad, N. Chaoui, M. Trzpit, N. Ghazzal, D. Robert, J.V. Weber, J. Photochem. Photobiol. A 183 (2006) 218–224.
[14] D. Robert, Catal. Today 122 (2007) 20–26.
[15] H. Fuji, M. Ohtaki, K. Eguchi, H. Arai, J. Mol. Catal. A: Chem. 129 (1998) 61–68.
[16] X. Mathew, J.P. Enriquez, A. Romeo, A.N. Tiwari, Sol. Energy 77 (2004) 831–838.
[17] K.K. Nanda, S.N. Sarangi, S. Mohanty, S.N. Sahu, Thin Solid Films 322 (1998) 21–27.
[18] X.Q. Li, Y. Cheng, L.F. Liu, J. Mu, Colloids Surf. A: Physicochem. Eng. Aspects 353 (2010) 226–231.
[19] C.F. Chi, Y.L. Lee, H.S. Weng, Nanotechnology 19 (2008) 125704–125705.
[20] X.X. Yang, C.D. Cao, L. Erickson, K. Hohn, R. Maghirang, K. Klabunde, J. Catal. 260 (2008) 128–133.
[21] M. Melle-Franco, M. Marcaccio, D. Paolucci, F. Paolucci, V. Georgakilas, D. Guldi, J. Am. Chem. Soc. 126 (2004) 1646–1647.
[22] D. Deutsch, J. Tara′bek, M. Krause, P. Janda, L. Dunsch, Carbon 42 (2004) 1137–1141.
[23] J. Chlistunoff, D. Cliffel, A.J. Bard, Thin Solid Films 257 (1995) 166–184.
[24] M.C. Buzzeo, R.G. Evans, R.G. Compton, Chem. Phys. Chem. 5 (2004) 1106–1120.
[25] R.C. Haddon, A.F. Hebard, M.J. Rosseinsky, D.W. Murphy, Nature (1991) 320–322.
[26] C.J. Brabec, N.S. Sariciftci, J.C. Hummelen, Adv. Funct. Mater. 11 (2001) 15–26.
[27] J.J. Davis, H.A.O. Hill, A. Kurz, A.D. Leighton, A.Y. Safronov, J. Electroanal. Chem. 429 (1997) 7–11.
[28] A. Szucs, A. Loix, J.B. Nagy, L. Lamberts, J. Electroanal. Chem. 397 (1995) 191–203.
[29] N. Nakashima, T. Ishii, M. Shirakusa, T. Nakanishi, H. Murakami, T. Sagara, Chem. Eur. J. 7 (2001) 1766–1772.
[30] S.U.M. Khan, M. Al-Shahry, W.B. Ingler, Science 297 (2002) 2243–2245.
[31] X.W. Zhang, M.H. Zhou, L.C. Lei, Carbon 43 (2005) 1700–1708.
[32] S.H. Kim, S.K. Lee, J. Photochem. Photobiol. A: Chem. 203 (2009) 145–150.
[33] H. Gerischer, M. Lubke, J. Electroanal. Chem. 204 (1986) 225–227.
[34] A. Maurya, P. Chauhan, Mater. Charact. 62 (2011) 382.
[35] M.A. Barakat, H. Schaeffer, G. Hayes, S. Ismat-Shah, Appl. Catal. B: Environ. 57 (2005) 23–30.
[36] J.C. Colmenares, M.A. Aramendia, A. Marinas, J.M. Marinas, F.J. Urbano, Appl. Catal. A 306 (2006) 120–127.
[37] Y. Liu, J.F. Ma, Z.S. Liu, C.H. Dai, Z.W. Song, Y. Sun, J.R. Fand, J.G. Zhao, Ceram. Int. 36 (2010) 2073–2077.
[38] Z.L. Liu, Z.L. Cui, Z.K. Zhang, Mater. Charact. (2005) 123–129.
[39] Z.D. Meng, M.L. Chen, F.J. Zhang, L.Z.J.G. Choi, W.C. Oh, Asian J. Chem. 23 (2011) 2327–2331.
[40] Z.D. Meng, J.G. Choi, W.C. Oh, Asian J. Chem. 23 (2011) 847–851.
[41] K. Kokubo, S. Shirakawa, N. Kobayashi, H. Aoshima, T. Oshima, Nano Res. 23 (2011) 847–851.
[42] X. Zhang, W. He, A. Zhao, H. Li, L. Chen, W.W. Pai, J. Hou, M.M.T. Loy, J. Yang, X. Xiao, Phys. Rev. B 75 (2007) 235444–235452.
[43] W.C. Oh, A.R. Jung, W.B. Ko, Mater. Sci. Eng. C 29 (2009) 1338–1347.
[44] R. Flood, B. Enright, M. Allen, S. Barry, A. Dalton, H. Doyle, D. Tynan, D. Fitzmaurice, Sol. Energy Mater. Sol. Cells 39 (1995) 83–98.
[45] C. Li, J. Yuan, B.Y. Han, L. Jiang, W.F. Shangguan, Int. J. Hydrogen Energy 35 (2010) 7073–7079.